# EXPERIMENTAL AND NUMERICAL INVESTIGATION OF TRANSONIC FLOW PAST A 2D TURBINE CASCADE

## *EXPERIMENTÁLNÍ A NUMERICKÝ ROZBOR TRANSSONICKÉHO PROUDĚNÍ VE 2D TURBÍNOVÉ MŘÍŽI*

J. Dobeš**, J. Fořt*, J. Fürst**, J. Halama*, T. Hyhlík**, P. Louda*, K. Kozel*, J. Příhoda*, P. Šafařík*

*Institute of Thermomechanics AS CR
Dolejškova 5, 182 00 Praha 8, Czech Republic

*Faculty of Mechanical Engineering, CTU Prague
Technická 4, 166 07 Praha 6, Czech Republic

## ABSTRACT

The paper deals with both experimental and numerical results of investigations into transonic flow past the SE 1050 turbine blade cascade. Empirical data set is a basis for testing of different research techniques. Experimental results namely results of optical measurements give information on flow structure in the transonic flow field and enable to evaluate quantitative data on flow parameters for comparison with results of independent methods. Numerical solutions of transonic flow past the SE 1050 turbine cascade are based on 2D inviscid, and 2D viscous turbulent flow models. Achieved numerical results by both in-house and commercial software are compared mutually and also with experimental data. The analysis of results by different numerical schemes, grid arrangements and boundary conditions is carried out.

## *ANOTACE*

*Příspěvek se zabývá jak experimentálními tak i numerickými výsledky rozboru proudění v turbínové mříži SE1050. Soubor naměřených dat je základem pro testování nejrůznějších vědeckých postupů. Experimentální výsledky, zejména výsledky optických měření poskytují informace o struktuře transsonického proudového pole a umožňují získat parametry proudu pro porovnání s výsledky nezávislých metod. Numerická řešení transsonického proudění v turbínové mříži SE1050 jsou založena na modelech 2D nevazkého a 2D vazkého turbulentního proudění. Numerické výsledky dosažené pomocí vlastních i komerčních programů jsou porovnány nejen navzájem, ale také s experimentálními daty. Rozbor výsledků dosažených pomocí různých numerických schémat, různých typů výpočtových sítí a různých okrajových podmínek je uveden. Uvedené výsledky numerických metod ukazují, že vyvinutý software je možné použít k numerické simulaci transsonického (nevazkého, vazkého turbulentního) proudění v rovinné lopatkové mříži.*

**Key words:** transonic flow, axial turbine, numerical solution, turbulent flow.

*Klíčová slova:* transsonické proudění, axiální turbína, numerické řešení, turbulentní proudění.

## 1. INTRODUCTION

Investigations in the field of transonic flow are still of great interest. Namely industry projects need reliable data on flow behavior and characteristics at high speeds of the working medium. The

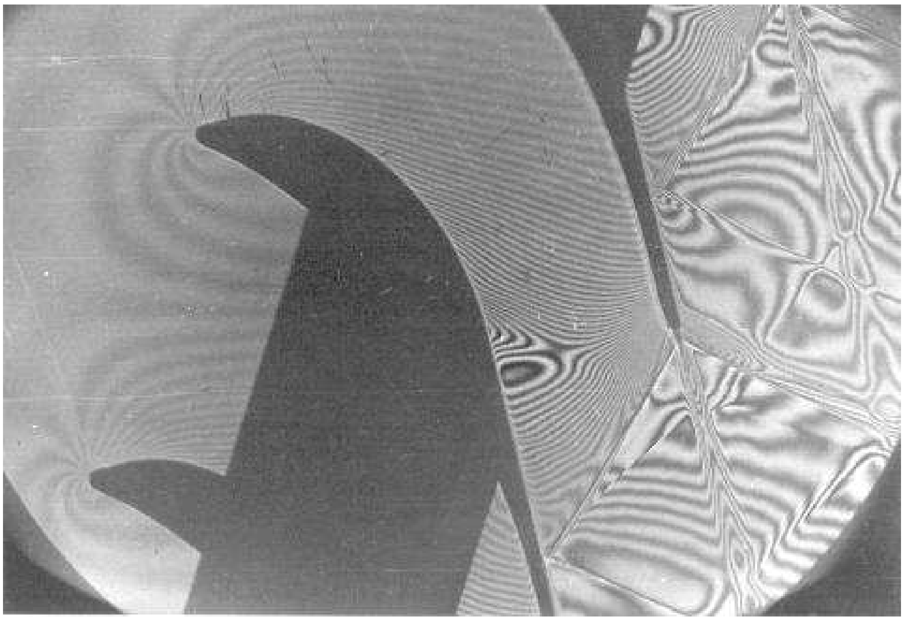

Figure 1: The interferometric picture of flow in the SE 1050 blade cascade (incidence angle $i = 0°$, isentropic exit Mach number $M_{2is} = 1.198$, inlet Mach number $M_1 = 0.375$)

aim of this paper is to present results from our common experimental and numerical aerodynamic research program and to perform detailed analysis and comparisons of results. The experiments were carried out in the High-Speed Aerodynamic Tunnel of the Institute of Thermomechanics, Academy of Sciences of the Czech Republic. Optical and pneumatic measurements were used. The numerical simulations were achieved by means of several numerical methods for computation of 2D flow through cascades. The methods were developed by the co-authors [1]. The commercial program FLUENT was applied [2] as well. The SE1050 turbine blade cascade [3] was investigated at transonic velocities. Interferometric measurements and numerically solved flow fields enable us to have an insight into transonic flow structure. The flow structure and flow phenomena are described. Quantitative data are evaluated and give a basis for comparison of results and for further analysis.

## 2. EXPERIMENTAL RESULTS

Transonic flow past profile blade cascades has the complex structure of the flow field especially in the exit part of turbine cascade. Interferogram in the Fig.1 presents transonic flow past the SE1050 turbine profile blade cascade for inlet angle 70.7°, isentropic exit Mach number $M_{2is} = 1.198$, and inlet Mach number $M_1 = 0.375$. The subsonic inlet flow is accelerated in the channels between profiles. Near the throat of the channel the velocity of sound is reached; from evaluation of the interferogram in the Fig.1 the sonic line can be identified at the coordinate $x/b = 0.40$ on the suction side, when $x$ is coordinate along the chord, $b$ is chord of the profile. The influence of the geometry of the channel throat and irreversible processes on the conditions of aerodynamic choking were studied in [4]. Further expansion into supersonic velocities leads to decrease and subsequent increase of the flow velocity on the suction side. We call this effect supersonic compression accompanying transonic expansion or recompression. It was shown [3] that the compression effect is directly related to the discontinuity of the curvature of the suction side surface at the coordinate $x/b = 0.5$, i.e. the point of velocity decrease. The intensive supersonic expansion in the exit part of the cascade is terminated by the inner branch of exit shock waves. The shock wave interacts with boundary layer and reflects from the suction side. The

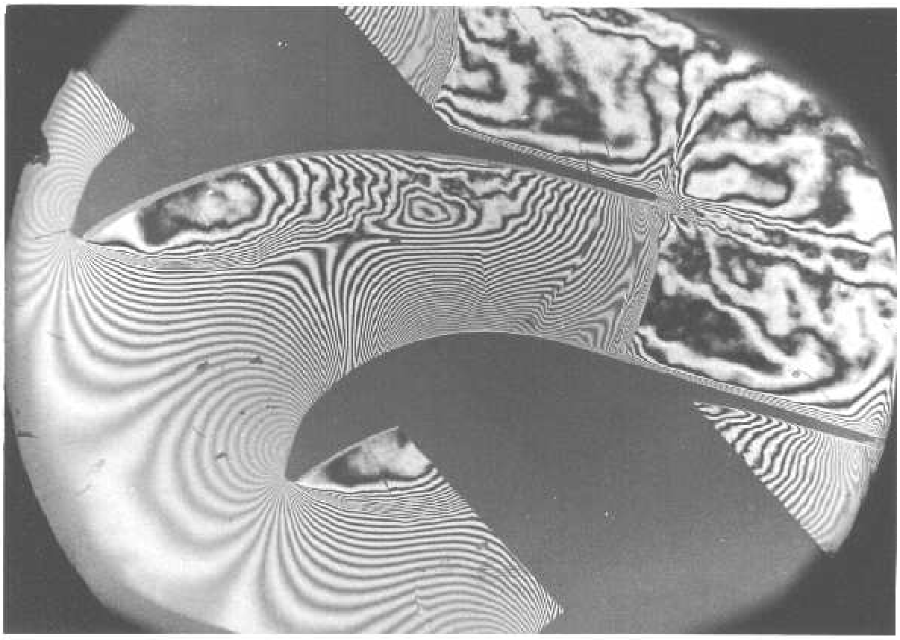

Figure 2: The interferometric picture of flow in the SE 1050 blade cascade (incidence angle $i = -67°$, isentropic exit Mach number $M_{2is} = 0.905$, inlet Mach number $M_1 = 0.545$)

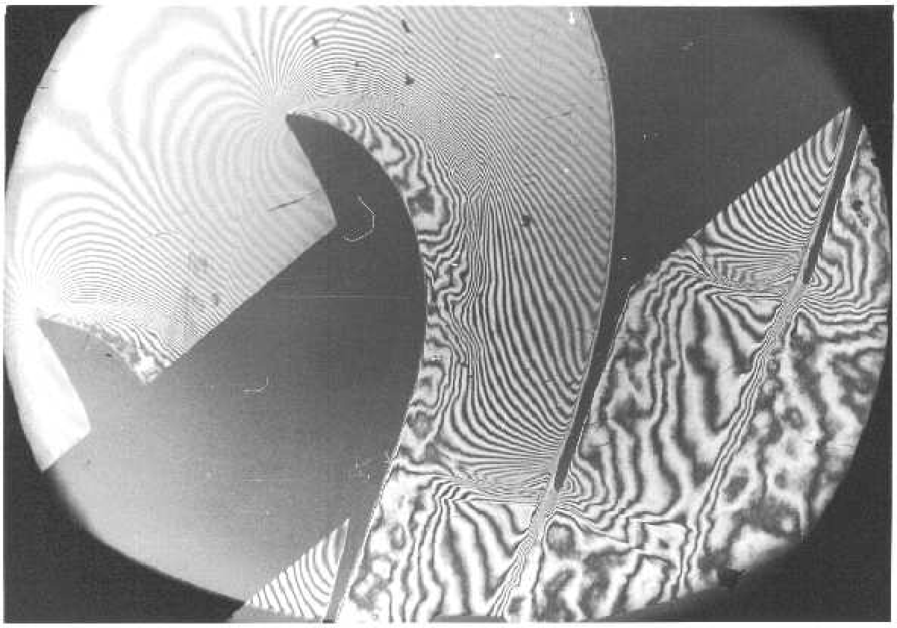

Figure 3: The interferometric picture of flow in the SE 1050 blade cascade (incidence angle $i = +30°$, isentropic exit Mach number $M_{2is} = 1.012$, inlet Mach number $M_1 = 0.660$)

experimental and numerical study of boundary layer development on the SE 1050 profile [5] proved the transition of laminar boundary layer to turbulent during the supersonic compression accompanying transonic expansion. This fact explains the typical turbulent structure of the interaction of boundary layer with the internal branch of exit shock waves. After the interaction the supersonic expansion is slowed down, to become again more intensive before the trailing edge. The supersonic flows on both suction and pressure side of trailing edge separate at points where lip shocks as a consequence of over-expansion appear. Downstream of the trailing edges the system of the exit shock waves and wakes forms. Wakes are relatively thin and both branches of exit shock waves are weakened by expansions upstream of the trailing edge. This complex transonic flow structure is analyzed, parameters of flow are evaluated, and data for comparison of results of independent investigation methods are prepared.

Figure 2 shows transonic flow through the SE 1050 blade cascade at a very small load (incidence angle $i = -67°$, isentropic outlet Mach number $M_{2is} = 0.905$, inlet Mach number $M_1 = 0.545$). The subsonic inlet flow is accelerated in the inter-blade channel to supersonic velocities. The potential flow region is terminated downstream by an intensive shock wave passing the inter-blade channel at neighboring profile trailing edge at the relative chord-wise coordinate on the suction side $x/b = 0.570$. The potential core is bounded by a boundary layer on the suction side of the profile and by a shear layer of the local flow separation on the pressure side of the profile. Due to a very small load of the SE 1050 blade cascade the leading edge separation occurs on the pressure side and the flow re-attaches to the pressure side in the vicinity of the local maximum of density at the pressure side at the relative chord-wise coordinate $x/b = 0.660$. In reference [6] a turbulent structure developing in the flow separation shear layer in the separation zone, in the re-attachment zone, on the pressure side upstream of the trailing edge and in the wake, particularly in its inner side towards the cascade was shown. The local supersonic region in the vicinity of the suction side of the profile trailing edge and the relatively wide wake are further transonic structures. The local maximum of density in the vicinity of pressure side is accompanied by a shear layer, which seems to be relatively stable. The strongly dissipative separation zone should be studied.

The interferogram in Fig.3 obtained at an extreme overload (incidence angle $i = +30°$, isentropic outlet Mach number $M_{2is} = 1.012$, inlet Mach number $M_1 = 0.661$) shows an extensive flow separation on the suction side of the leading edge. However, the separation does not reach the cascade exit. An approximate point of the shear layer re-attachment on the suction side can be identified at the relative chord-wise coordinate about $x/b = 0.320$, but the interferogram shows that this layer has a wave (and probably unsteady) character in the whole area and it influences the flow field in the entire inter-blade channel and farther downstream. The expansion into supersonic velocities at the trailing edge can be observed. An interaction between the shock wave and the intensive dissipative layer on the suction side is evident. The one-sides wake is anomalous and should be noticed.

The traversing probe method makes it possible to derive, using integral balancing of the mass, momentum and energy of the flow, the referential conditions at the outlet of the cascade and determine the basic flow characteristics : the outlet flow angle and the kinetic energy loss coefficient. The kinetic energy loss coefficient is defined by $\zeta = 100\left(1 - \frac{\lambda_2^2}{\lambda_{2is}^2}\right)$ [%], where $\lambda_2$ is exit relative velocity (the ratio of the given and critical velocity) and $\lambda_{2is}$ is isentropic exit relative velocity. The kinetic energy loss coefficient in vicinity to the nominal operation mode (Fig.1) was measured several times and is $\zeta = 4.6\%$ according to [2], $\zeta = 4.24\%$ and $\zeta = 4.79\%$ according to [7]. Extreme values of the incidence angles cause flow separation on the leading edge of the blade. The separation results in significant increase of the kinetic energy loss coefficient. It is for the regime at part load (Fig.2) $\zeta = 15.9\%$ and for the regime at overload $\zeta = 10.2\%$ [6].

## 3. NUMERICAL SOLUTION

The flow in SE 1050 turbine cascade at the design conditions (Fig.1) has following features: thin boundary layers without earlier separation in front of trailing edge, large parts of laminar boundary layer along profile surface, thin wake, position of sonic line between blade surfaces. These physical properties give us opportunity to consider some simplified flow models and compare some flow field phenomena with experimental data. This is very important for investigation of typical properties of numerical methods by numerical experiments. Some features, which can be easily detected for simplified flow models, could be hardly determined for complex flow models, though they are still present (e.g. non-physical production of entropy near the leading edge of profile).

### Governing equations

We consider 2D Navier-Stokes equations (1) for the perfect gas.

$$\mathbf{W}_t + \mathbf{F}_x + \mathbf{G}_y = \frac{1}{Re}(\mathbf{R}_x + \mathbf{S}_y), \tag{1}$$

where

$$\begin{aligned}
\mathbf{W} &= [\rho, \rho w_1, \rho w_2, e]^T \\
\mathbf{F} &= [\rho w_1, \rho w_1^2 + p, \rho w_1 w_2, w_1(e+p)]^T \\
\mathbf{G} &= [\rho w_2, \rho w_2 w_1, \rho w_2^2 + p, w_2(e+p)]^T \\
\mathbf{R} &= [0, \tau_{11}, \tau_{12}, w_1\tau_{11} + w_2\tau_{12} + \frac{\lambda}{Re}\frac{\partial T}{\partial x}]^T \\
\mathbf{S} &= [0, \tau_{21}, \tau_{22}, w_1\tau_{21} + w_2\tau_{22} + \frac{\lambda}{Re}\frac{\partial T}{\partial y}]^T \\
\tau_{ij} &= \eta\Big(\frac{\partial w_j}{\partial x_i} + \frac{\partial w_i}{\partial x_j} - \frac{2}{3}\delta_{ij}\frac{\partial w_j}{\partial x_j}\Big) \\
Re &= \frac{w^* L^* \rho^*}{\eta^*}
\end{aligned}$$

The symbol $\rho$ denotes density, $w_i$ are the Cartesian components of a velocity vector, $e$ is a total energy per unit volume, $p$ is a static pressure and $\kappa$ is the ratio of specific heats. The superscript $^*$ is used for reference quantities, $\tau_{ij}$ are shear stresses, $Re$ is the Reynolds number, $\lambda$ is a thermal conductivity and $\eta$ is a viscosity coefficient. The system of equations is closed by the equation for the pressure of the perfect gas (2)

$$p = (\kappa - 1)[e - \rho\,\frac{w_1^2 + w_2^2}{2}]. \tag{2}$$

We suppose $\eta = 0$ for the case of an inviscid flow (Euler equations). The same form of governing equations is considered for time averaged values (RANS), then $\eta = \eta_{laminar} + \eta_{turbulent}$ and the Prandtl number is modified similarly.

### Mathematical formulation

The domain of solution $\mathcal{D}$ consists of one cascade pitch. A solution $\mathbf{W}$ has to fulfill the integral form (3) of Eq. (1) inside any domain $D \subset \mathcal{D}$ with a sufficiently smooth boundary and boundary conditions along $\partial D$

$$\int_{t_1}^{t_2}\iint_D \Big(\mathbf{W}_t + \mathbf{F}_x + \mathbf{G}_y - \frac{1}{Re}(\mathbf{R}_x + \mathbf{S}_y)\Big)\,dV\,dt = 0. \tag{3}$$

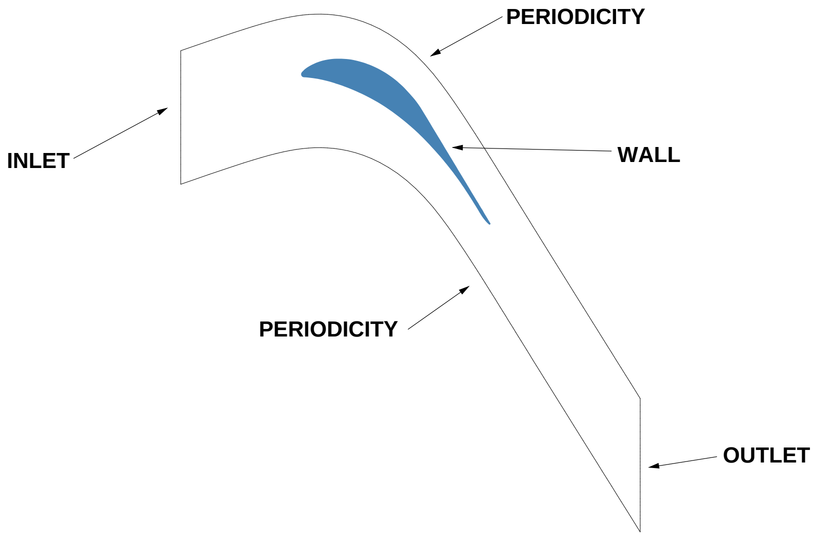


Figure 4: Axial plane cascade - computational domain.

The non-permeability condition $\vec{w} \cdot \vec{n} = 0$ ($\vec{n}$ denotes the unit vector perpendicular to the wall) is prescribed along walls - see Fig. 4 - for an inviscid flow model, whereas the no-slip condition ($\vec{w} = \vec{0}$) and the adiabatic wall condition are used for a viscous flow model. The stagnation values of the density $\rho_0$ and the speed of sound $a_0$ and the velocity angle $\alpha$ are imposed at the inlet. The pressure is prescribed at the outlet. The periodicity of all components of $\mathbf{W}$ is considered along upper and lower boundary of computational domain (Fig. 4).

### Numerical Methods

A numerical solution has been performed by several numerical methods. On a structured grid we use three Lax-Wendroff type schemes: the full TVD and the Causon simplified form of TVD MacCormack scheme (Fürst and Kozel [12]) and cell-vertex scheme (e.g. Stringer and Morton [11], Dobeš et al [10]) with several modifications of artificial dissipation. Next the implicit upwind method based on AUSM U scheme, MUSCL reconstruction along grid lines and van Leer's limiter has been developed. The other upwind methods are based on approximate Riemann solver (Roe, Osher), a proper reconstruction (WENO, MUSCL or central least squares with van Leer's or Barth's slope limiter ) and explicit as well as implicit forms in time variable. They have been used on generally unstructured grids. The approximation of viscous fluxes is always finite volume central approximation second order, its details depends on the type of finite volume.

### Grids

Several types of 2D grids have been used and tested for inviscid flow model. Simple algebraically generated structured H-type grid, curvilinear elliptically generated H-type grid, multi-block O-H grid and unstructured triangular grid (with or without adaptation) - see leading and trailing edge details in Fig. 5.

Results of computations of an inviscid flow in SE1050 turbine cascade showed the influence of grid (especially the leading and the trailing edge discretization can significantly affect the quality of a numerical solution) see [1]. A strong entropy production near leading edge and entropy layer

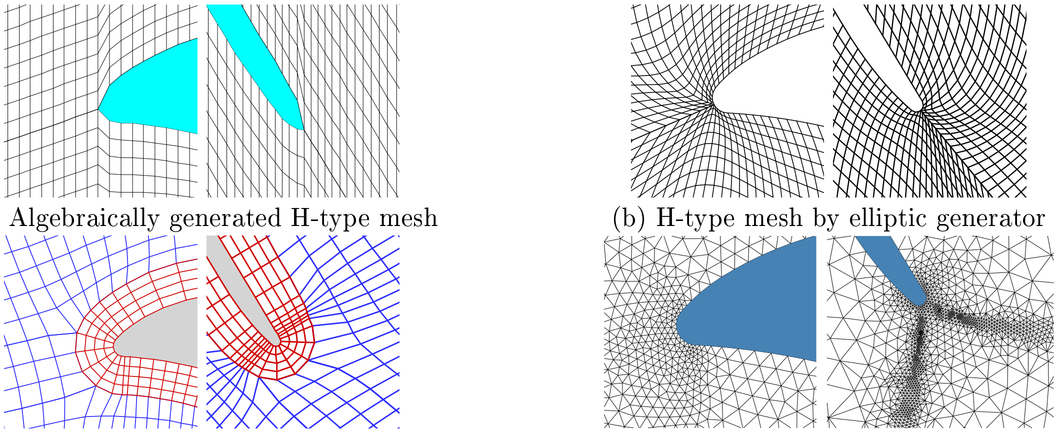

(a) Algebraically generated H-type mesh (b) H-type mesh by elliptic generator

(c) O-H structured multi-block mesh (d) Adapted triang. unstructured mesh

Figure 5: Leading and trailing edge discretization – axial cascade SE1050

downstream the trailing edge is typical for simple H-grid (Fig. 5 a ). This is improved using either the structured O-H multi-block grid or the unstructured triangular grid (Fig. 5 c, d ). They are both grids with rapid coarsening of grid cells behind the trailing edge. The entropy production near leading edge was effectively suppressed also by elliptical H - type grid, but the an entropy layer behind the trailing edge remained, i.e. it is not the leading edge grid effect, but trailing edge grid feature.

This type of grid has been used for all computations of viscous flow through cascade with proper refinement of grid near walls and in the wake region. Some grid effects will be discussed in the next section.

### Turbulence models

We used the following types of turbulence models:

- algebraic Baldwin - Lomax model with or without prescribed (forced) transition [15], [16] ;
- a one equation Spalart-Allmaras model [9];
- a two equation SST and modified SST models [8];
- the following models implemented into commercial software Fluent : Spalart-Allmaras, RNG $k-\epsilon$.

## 5. SOME NUMERICAL RESULTS

### Laminar flow through axial cascade SE1050

A natural continuation in development of numerical method validated for inviscid transonic flow is its extension and validation for laminar and then for turbulent transonic high Reynolds number flows. Although the laminar flow model is artificial for high Reynolds numbers, its numerical solution can show the applicability of methods for high Reynolds number flow calculations (and it is not automatically true for any method suitable for computation of inviscid transonic flow) . Also the grid quality must be tested.

A good discretization of leading edge region is at least as important as for inviscid flow calculations. The viscous effect near the wall (boundary layer), trailing edge (wake) and for transonic flow very important phenomenon of shock wave - boundary layer and shock wave - trailing edge - wake interaction (lip shock structure) must be numerically captured. And it of course needs a proper grid refinement.

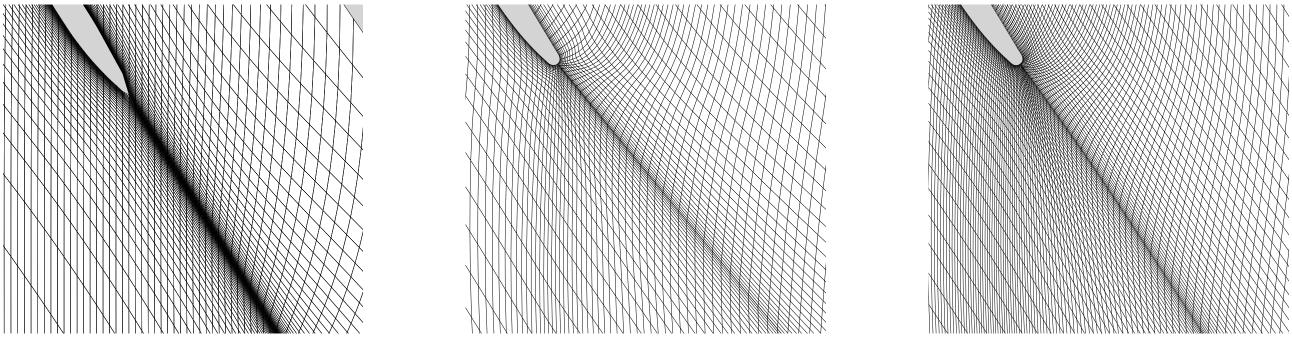

(a) algebraic H-type grid (b) elliptic H-type grid (c) elliptic H-type grid

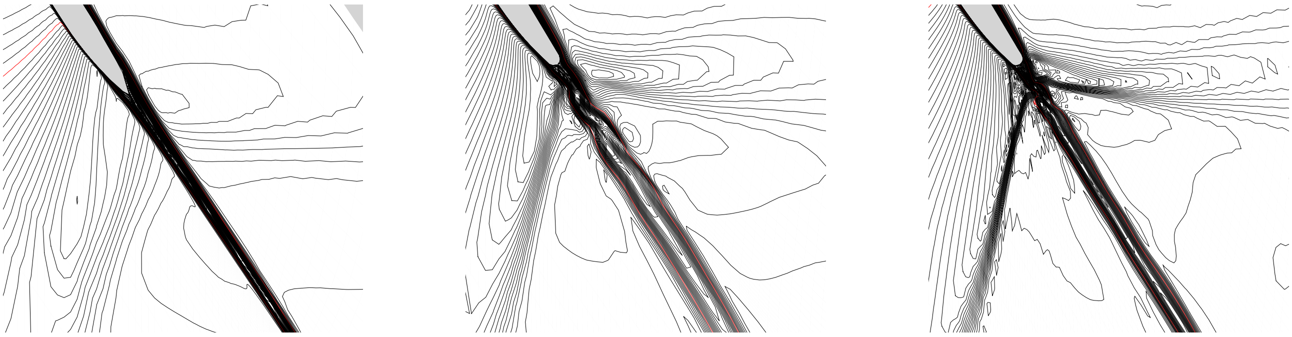

(d) explicit MUSCL (Roe) method on grid (a) (e) cell-vertex method on grid (b) (f) cell-vertex method on grid (c)

Figure 6: Laminar flow - influence of discretization of trailing edge region

Figure 6 shows laminar flow in the vicinity of trailing edge and in the wake and its dependency on a grid quality. Figure 6(a) (inappropriately refined grid, Roe high resolution scheme) shows a steady wake and bad resolution of a shock wave structure. Better discretization of the trailing edge in Fig. 6(b) provides an unsteady wake and further refined grid in Fig. 6(c) even captures shock wave structure comparable with experimental data (lip shocks). These results has been computed by cell vertex scheme. We can see from the shape of isolines in Fig. 6(c), that the artificial viscosity coefficients are on the lowest possible level. Some phenomena in Fig. 6 can be compared with the experimental data. The analysis of experimental results [5], see Fig. 1, shows that the boundary layer is laminar along the whole pressure side. On the suction side it is laminar up to re-compression domain and after short transition becomes turbulent. Therefore some phenomena in Fig. 6 can be directly compared with the experimental data, like lip shock structure. The thickness of computed boundary layer must be comparable with experimental data on the pressure side of profile and lower on suction side. The same is true for the wake. The physics of laminar boundary layer - shock wave interaction is different as for turbulent boundary layer - shock wave interaction (e.g. in Fig.1). The laminar boundary layer is thicker in the place of incoming shock wave. There is a local separation bubble (with re-attachment). The shock reflexion has therefore a typical structure, which stream-wise consists of first reflected shock wave in front of bubble, expansion waves from the top of bubble, second reflected shock wave behind the bubble. We can see in Fig.7, that sufficiently fine grid also in stream-wise direction with proper aspect ratio of grid cells near the wall is necessary to capture this phenomenon correctly.

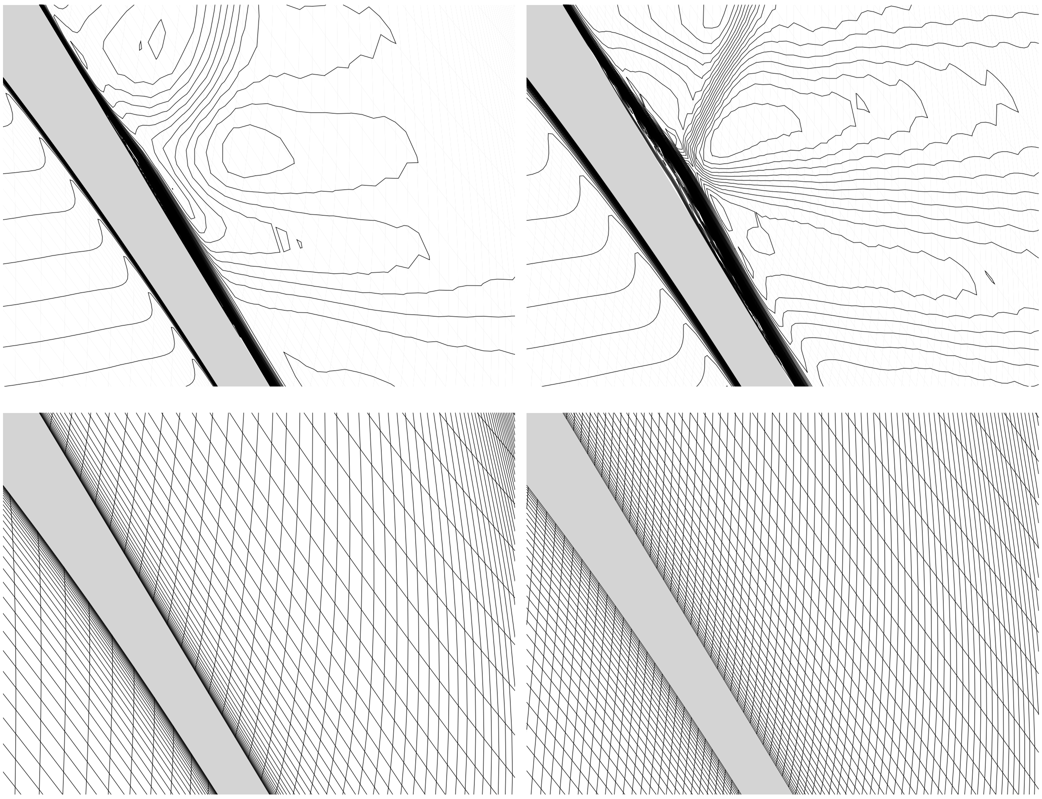

Figure 7: Shock-laminar boundary layer interaction

**Turbulent flow through axial cascade SE1050**

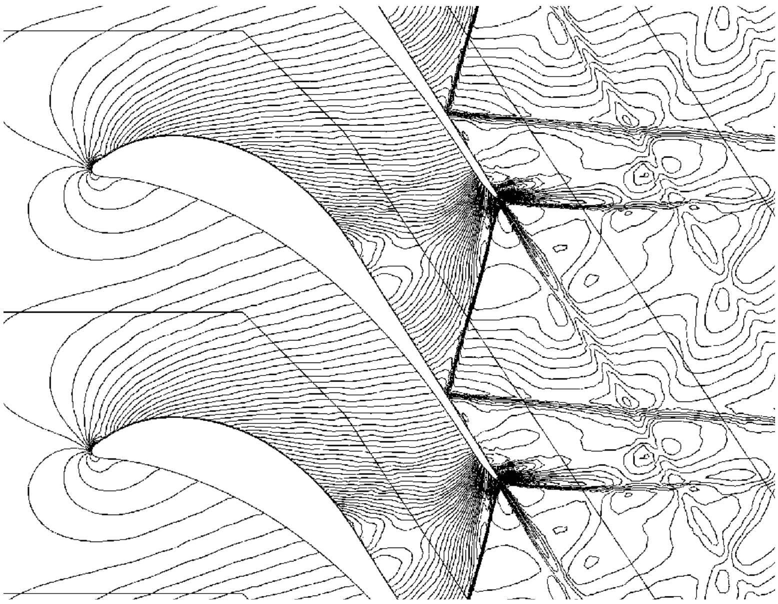

Figure 8: Isolines of density. Results of commercial software FLUENT.

Results achieved by the commercial software FLUENT (RNG $k-\epsilon$ turbulence model with wall functions ) are plotted in a form of density isolines in Fig. 8. The main features of flow field are well captured. The numerical aproximation of outlet boundary condition in FLUENT is not suitable for transonic flow. We can observe a shock reflected as an expansion wave from the outlet boundary. These expansion waves travel back, interacting with original shock structure and reach also the area of blade channel and suction side of profile. This phenomenon affects shock wave structure, distribution of pressure along profile, wake structure and consequently also level of losses.

The best elliptic H type grid from comparisons presented in previous paragraph has been used for computations of turbulent flow by in-house developed methods. The quality of grid refinement near wall was additionally tested, to ensure that at least first two grid points are located in part with $y^+ < 5$.

The high resolution Roe scheme with MUSCL reconstruction has been used for solution of inviscid, viscous laminar and turbulent flow with Baldwin - Lomax model of turbulence.

Fig. 9 shows the pressure distributions along profile from inviscid, laminar (Fig. 10(a)) and turbulent (Fig. 10(b)) flow models and from the experiment. The graphs for different flow models are very similar. Therefore in this case also inviscid flow model is able to capture main flow features. On the other hand it is evident that only pressure distribution along the profile is not sufficient for the quality evaluation of numerical results of other flow models.

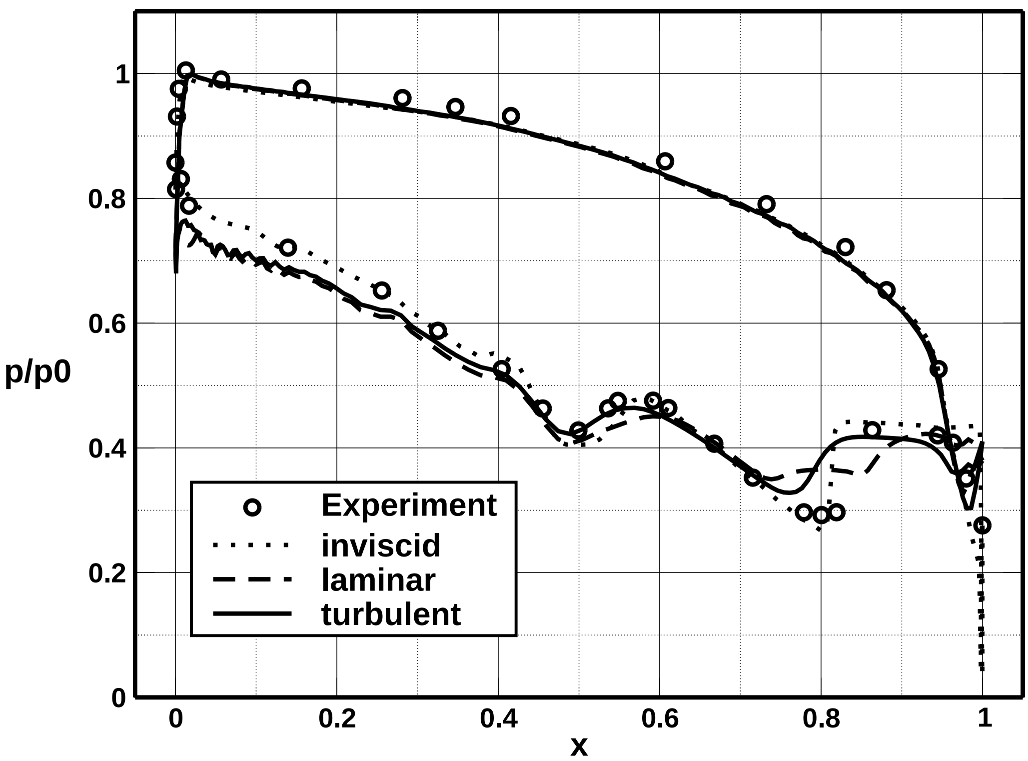


Figure 9: SE1050, explicit MUSCL (Roe), Mach number distribution along profile for different flow models

Also a turbulent flow model (Baldwin-Lomax), when used for the whole flow field, does not fit completely the conditions of experiment. Fig. 10 compares results achieved by a laminar and a turbulent flow models and a turbulent flow model with the forced transition - the onset and the offset of transition is set according to experimental data (the onset on the suction side is marked by arrow in Fig. 10(c), the transition region is very short, the flow along the whole pressure side is laminar) .

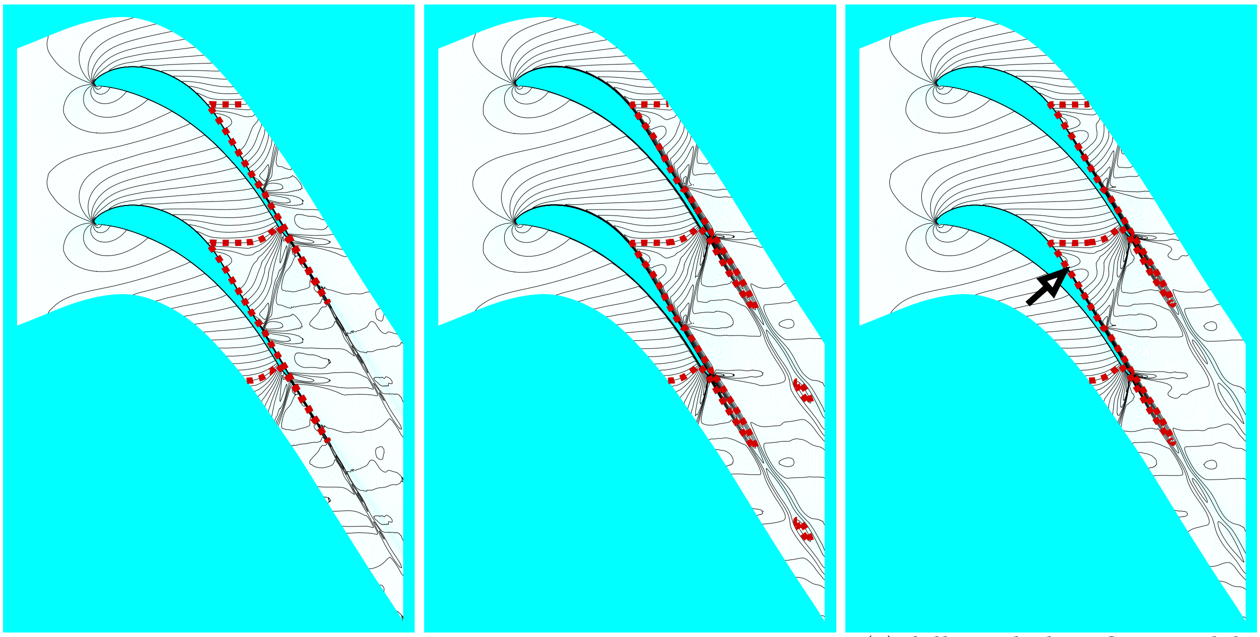

(a) laminar flow model

(b) fully turbulent flow model

(c) fully turbulent flow model with forced transition, arrow shows the transition onset

Figure 10: Flow in SE1050, explicit MUSCL (Roe) method, isolines of Mach number (marks denote the sonic line, $\Delta M = 0.05$).

Fully turbulent computation shows too thick boundary layer e.g. on the suction side. The boundary layer thickness becomes smaller, when the laminar part is taken into account, see Fig. 10(c).

The important boundary layer and shock wave structures are compared in a zoom of part of computed flow field in Fig. 11. We can compare difference between laminar (a) and turbulent (b,c,d) boundary layer - shock wave interaction on the suction side of profile. Next we can see very thin boundary layer and wake computed by laminar flow model (a) and contrary too thick boundary layer and wake computed by Baldwin - Lomax without transition (b). The results (c) and (d) has been computed by Baldwin - Lomax turbulence model with forced transition. It means that the turbulent viscosity coefficient along each grid line crossing the profile surface has been multiplied by the weight (like intermittency) function $\Phi$. We put $\Phi = 0$ in front of transition onset, $\Phi = 1$ in fully turbulent part and $\Phi$ is a monotone increasing function with values in $\langle 0, 1 \rangle$ in transitional region. The position of transition region was prescribed according to experimental data analysis for case (c). These results agrees best to experimental data. The position of transitional region in Fig.11 (d) was prescribed according to results of 1D boundary layer computation for given outer velocity (pressure) distribution and prescribed level of inlet turbulence intensity equal to values common in last low pressure turbine stage (about 3% ). It is more than 10 times higher, than for wind tunnel measurement. The position of transition region is therefore shifted upstream. Comparison of case (c) and (d) shows the importance of its position.

Results presented in Fig.12 has been computed on the same grid by implicit AUSM U scheme (linear MUSCL reconstruction, van Leer limiter) and two equation SST model. There is no model of transition. We can see again a good agreement with the experimental data, all important phenomena in flow field are captured. The boundary layer is thinner than in Fig.10.

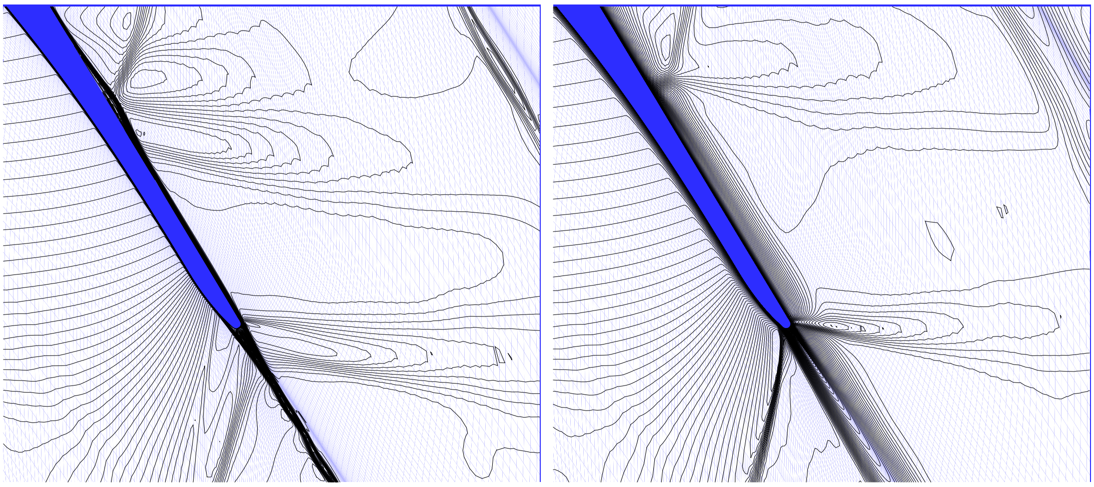

(a) laminar flow model (b) Baldwin - Lomax turbulent flow model

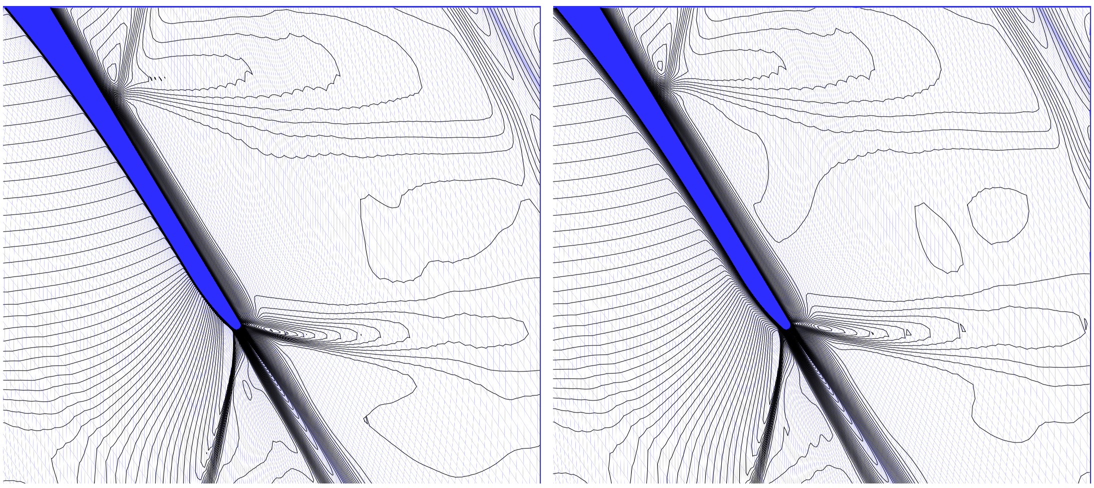

(c) forced transition according experiment (d) forced transition -different case

Figure 11: Detail of flow field

The next Fig.13 compares pressure distribution along profile computed by different turbulence models and numerical schemes. We can see, that some differences are visible near shock wave on the suction side of profile. The shock wave position is best captured by SST model - AUSM U scheme, but only the B-L model - Roe scheme with forced transition gives sufficiently sharp shock. The smeared shock in the other compared computations in Fig.13 is a consequence of the influence of viscosity (and a boundary layer thickness). The viscosity consists of laminar viscosity (given Reynolds number), turbulent viscosity (given by turbulence model) and numerical viscosity (given by scheme and grid). To distinguish the role of these components needs a lot of work in future. The Table 1 compares losses achieved by different methods. They were evaluated by the same procedure like for experimental data. Agreement among computed results is better than between experiment and numerics (numerical methods underpredict losses).

## 6. CONCLUSIONS

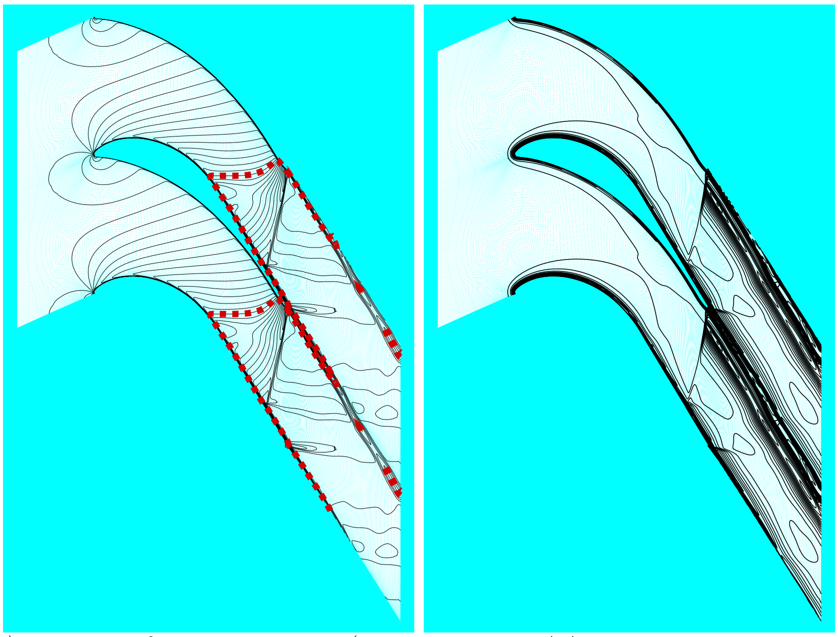

(a) isolines of Mach number (marks denote the sonic line, $\Delta M = 0.05$).

(b) isolines of turbulent viscosity.

Figure 12: Flow in SE1050, SST turbulence model, AUSM U method, isolines of Mach number (marks denote the sonic line, $\Delta M = 0.05$), the same elliptic H-type like for computations in Fig.10.

| Numerical method | turbulence model | losses |
|---|---|---|
| Experiment | | 4.5% |
| Roe RS, MUSCL, van Leer's limiter | Baldwin-Lomax turbulent | 4.0% |
| Roe RS, MUSCL, van Leer's limiter | Baldwin-Lomax transition | 3.3% |
| Roe RS, Lest Squares, Barth's limiter | Spalart-Allmaras | 3.4% |
| AUSM U, MUSCL, van Leer's limiter | SST model | 3.0% |

Table 1: Comparison of losses.

The extensive experimental and numerical research program on the SE 1050 profile cascade yielded information on the structure an d parameters of flow field. The experimental results of nominal operation regime and extreme operation modes are described in detail. Successful prediction of flow parameters important for technical evaluation by means of numerical methods requires such methods, which are able to capture all significant phenomena. Their quality depends on a discretization of convective terms, on a grid type and on an appropriate flow model. Particular care is necessary for the solution of relatively complex problems (grid quality) and when using a commercial software (appropriate formulation and numerical approximation of boundary conditions). Presented numerical results show that the developed numerical methods are able to solve transonic flow fields in blade cascades. Also an inviscid flow model (together with the boundary layer calculation) can yield information important for the design of turbine blading. The model of turbulence, numerical scheme for convective terms and grid inseperably influence the quality of numerical results. Therefore the amount of achieved results still does not allow to draw final conlusions about the properties of turbulence model in computed case of transonic flow in turbine cascades. Preliminary we can conclude that algebraic model of turbulence must be used together with a proper prediction of transition. The other used turbulence models yield comparable results without any special care about position of

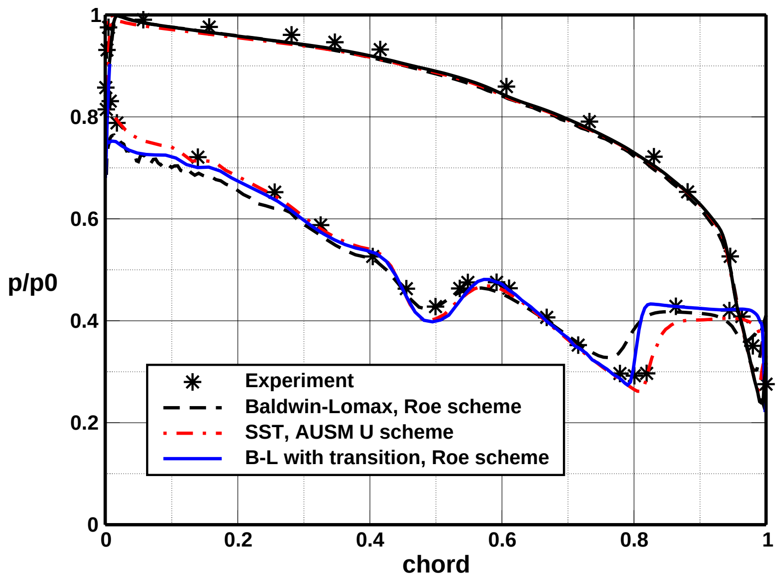


Figure 13: Pressure distribution along profile.

transitional region. Transonic flow regimes are very sensitive, therefore a successful prediction of flow characteristics by a numerical simulation is not simple and comparison with experimental data is appropriate for numerical method development.

## ACKNOWLEDGEMENTS

This work is supported by the grant AV CR No. IBS2076352 of the Academy of Sciences of Czech Republic, by the grants No. 101/02/0647, No. 201/02/0684 and No. 101/00/1057 of the Grant Agency of Czech Republic and by the Research Plan of MŠMT No. MSM/212200009.

## REFERENCES

[1] Dobeš J., Fořt J., Fürst J., Halama J., Kozel K.: Numerical solution of transonic flows in 2D and 3D axial and radial turbine cascades, pp 1105-1114, TURBOMACHINERY - Fluid Dynamics and Thermodynamics, Conference Proceedings, Prague, 2003.

[2] Fialová M., Hyhlík T., Kozel K., Šafařík P.: Numerical analysis data on the transonic flow past the profile cascade SE 1050, pp 45-48, Topical Problems of Fluid Mechanics 2001, Proceedings, Prague, 2001.

[3] Šťastný M., Šafařík P.: Experimental analysis data on the transonic flow past a plane turbine cascade, ASME Paper No.90-GT-313, New York, 1990.

[4] Macek J., Polášek M., Hyhlík T., Šafařík P.: 1-D model of flow past a nozzle considering losses and its simulations, pp 57-60 (in Czech), Topical Problems of Fluid Mechanics 2002, Proceedings, Prague, 2002.

[5] Šťastný M., Šafařík P.: Boundary layer effects on the transonic flow in a straight turbine cascade, ASME Paper No.92-GT-155, New York, 1992.

[6] Šťastný M., Šafařík P., Hořejší I., Matas R.: Flow around the sections of rotor blading of a turbine stage with relatively long blades at off-design conditions, Journal of Power and Energy, Vol.211, No.3, 1997, pp 207-213.

[7] Hyhlík T., Šafařík P.: A contribution to numerical result analysis of transonic flow field solutions, pp 55-60 (in Czech), 20th International Conference of Departments of Fluid Mechanics and Thermomechanics, Proceedings of the Conference, Ostrava, 2001.

[8] Menter F.R.: Two-equation eddy-viscosity turbulence models for engineering applications, AIAA Journal, Vol. 32, pp 1598-1605, 1994.

[9] Spalart P.R., Allmaras S.R.: A one equation turbulence model for aerodynamic flow, AIAA Paper No.92-439, 1992.

[10] Dobeš J., Fořt J., Fürst J., Halama J., Kozel, K.: Numerical simulation of a flow for turbomachinery applications, Internal flows, vol. 1, ed. P. Doerfer, Proceedings of 5th Int. Symp. on Experimental and Computational Aerothermodynamics of Internal Flows, IFFM Pub. 2001, ISBN 83-88237-35-7, pp 297-304.

[11] Stringer S.M., Morton K.W.: Artificial viscosity for the cell vertex method, Report no. 96/08, Oxford University Computing Laboratory, April 1996

[12] Fürst J., Kozel K.: Numerical solution of inviscid and viscous flows using modern schemes and quadrilateral or triangular mesh, Mathematica Bohemica, vol. 126, no. 2, 2001, pp 379-393 Braunschweig 1989, Vieweg, pp 63–74

[13] Angot P., Fürst J., Kozel K.: TVD and ENO schemes for multidimensional steady an unsteady flows – a comparative analysis, Proc. Finite Volumes for Complex Applications – Problems and Perspectives, editors: Benkhaldoun F., Vilsmeier R., Rouen 1996, Hermes, pp 283-290

[14] Fořt J., Fialová M., Fürst J., Horák M., Kozel K.: Numerical solution of several 2D and 3D internal flow problems, Proceedings of 15th International Conference on Numerical Methods in Fluid Dynamics, Monterey, USA, eds. P. Kutler, J. Flores, J.-J. Chattot, Springer-Verlag, Berlin 1997, pp 364-369

[15] Baldwin B., Lomax H. Thin Layer Approximation and Algebraic Model for Separated Turbulent Flows. AIAA paper 78-257. 1978

[16] Rostand P. Algebraic Turbulence Models for the Computation of Two-Dimensional High Speed Flows Using Unstructured Grids. NASA CR-181741. 1988